(Proceedings ModelCARE2011 held at Leipzig, Germany, in September 2011) (IAHS Publ. 355, 2012).

Comparison of equations of state for carbon dioxide for numerical simulations

NORBERT BÖTTCHER[1], JOSHUA TARON[2], OLAF KOLDITZ[1,2], RUDOLF LIEDL[1] & CHAN-HEE PARK[3]

1 Technische Universität Dresden, Helmholtzstr. 10, 01062 Dresden, Germany
norbert.boettcher@tu-dresden.de

2 Helmholtz-Centre for Environmental Research – UFZ, Permoserstr. 15, 04318 Leipzig, Germany

3 Korea Institute of Geoscience and Mineral Resources (KIGAM), 124 Gwahang-no, Yuseong-gu, Daejeon 305-350, Korea

Abstract In this work, we compare four equations of state for carbon dioxide with a large number of measurement data taken from literature. This comparison showed that complex equations of state are more accurate than simple ones. To see if the differences in accuracy have an influence on numerical simulations, we implemented the equations in the scientific software OpenGeoSys and performed comparative simulations of a compressible gas flow scenario. We found out that the difference between ideal gas and real gas behaviour is quite large, but the differences among the real gas equations have no significant influence on the simulation results.

Key words equation of state; compressible fluid flow; carbon dioxide; numerical simulation; gas storage; supercritical fluid

INTRODUCTION

Equations of state (EOS) are of major importance for the determination of fluid properties. Numerical simulations of gas-related applications such as carbon dioxide capture and storage (CCS) or natural gas storage (NGS) require the consideration of variable fluid properties. The volume of gases strongly depends on the system pressure and temperature conditions.

In fluid transport property correlations, i.e. viscosity or thermal conductivity, density has been chosen by many authors to be the significant argument (Stephan *et al*., 1987; Younglove & Ely, 1987; Vesovic *et al*. 1990; Fenghour *et al*., 1998). Furthermore, the density of a fluid is necessary to determine quantities such as compressibility, hydraulic conductivity, thermal diffusivity, or fugacity. Several EOS have been presented since van der Waals introduced the first equation to determine real-gas behaviour in 1873. In this article we compare four equations of state with a large number of measurement data. We selected popular formulations as examples for the common types of EOS (cubic, virial, and fundamental equations). In addition to the ideal gas law, i.e. the thermal equation of state for the hypothetical ideal gas, we chose the formulations of Peng & Robinson (1976), Duan *et al*. (1992), and Span & Wagner (1996) for comparison. While the first equation is suitable for most single-component systems, the latter two formulations had to be tuned to individual substances by a large number of fitting parameters. In our work, we use carbon dioxide as an example fluid.

In the first part of this paper, we use the datasets of density measurements performed by 14 different authors and compare them to the output of the selected EOS (see Table 1). This comparison indicates the accuracies of the different formulations at each state of aggregation.

The second part of the paper provides numerical comparative example simulations using all four EOS. Therefore, we implemented the equations of state and a PDE for compressible fluid flow in porous media into the open-source scientific software OpenGeoSys OGS (Böttcher *et al*., 2011; Park *et al*., 2011; Wang *et al*., 2009). The one-dimensional numerical example simulates a gas flow process, where turbulences or non-isothermal effects due to gas expansion are neglected. The example investigates the sensitivity of the model to the density function and shows the importance of the accuracy of the chosen EOS. In this analysis, we constrain our investigation on the influence of density and compressibility accuracy.

EQUATIONS AND COMPARISON

The most classic EOS is the equation of state for ideal gases. At standard pressure and temperature conditions, some fluids, e. g. CO_2, behave according to this formulation. In general, the higher the temperature and the lower the pressure, a fluid approaches to ideal behaviour (compare Fig. 1). The EOS for ideal gases can be written as:

$$pv_m = RT \tag{1}$$

where p is pressure, v_m is molar volume, R is the universal gas constant with R = 8.31451 J mol^{-1} K^{-1} (Cohen & Taylor, 1986), and T is temperature. For larger pressures (or lower temperatures), the gas behaviour according to system conditions may deviate from ideal behaviour. This deviation can be determined by using an EOS for real gases. The Peng & Robinson EOS (PR-EOS) is a van der Waals-type EOS since it uses the same approach to describe real gas behaviour. It uses two parameters a and b to describe attractive and repulsive forces between the gas molecules and is defined as:

$$p = \frac{RT}{v_\mathrm{m} - b} - \frac{a(T)}{v^2 + 2bv_\mathrm{m} - b^2} \tag{2}$$

with

$$a(T) = 0.45724\frac{R^2T^2}{p_c}\cdot\left[1+\kappa\left(1-T^{1/2}{}_r\right)\right]^2 \text{ and } b = 0.0778\frac{RT_c}{p_c} \tag{3}$$

In equation (3), κ is an empirical parameter given by $\kappa = 0.37464 + 1.54226\omega - 0.26992\omega^2$; ω is the acentric factor presented by Pitzer (1939) and indicates the deviation of the molecule shape from an ideal sphere. For CO_2, it can be determined to $\omega = 0.2249$. T_c and T_r are critical and reduced temperature, where $T_r = T_c/T$. PR-EOS can be rewritten into a third-degree polynomial, thus it belongs to the group of cubic EOS and therefore can be solved directly (e.g. using Cardano's method) so it is very fast to solve. A more complex EOS has been presented by Duan *et al*. (1992) which use 15 parameters to fit the equations outcome to real gas behaviour. The equation is known as Duan-Møller-Weare (DMW-EOS) and reads:

$$\frac{pv_\mathrm{m}}{\mathrm{RT}} = 1 + \frac{B}{V_r} + \frac{C}{V^2{}_r} + \frac{D}{V^4{}_r} + \frac{E}{V^5{}_r} + \frac{F}{V^2{}_r}\left(\beta + \frac{\gamma}{V^2{}_r}\right)\exp\left(-\frac{\gamma}{V^2{}_r}\right) \tag{4}$$

where

$$V_r = \frac{v_\mathrm{m} p_c}{RT_c} \tag{5}$$

The parameters B to F in (4) are called virial coefficients and are defined in Duan *et al*. (1992). Unlike PR-EOS, these parameters have no physical meaning. They have to be tuned using measurement data. The equation of state presented by Span & Wagner (1996) is based on the fundamental equation of thermodynamics. It is a semi-analytical approach and has been fitted to real CO_2-behaviour by employing a large number of fitting parameters. The formulation uses a derivation of the Helmholtz energy equation to predict the density of the fluid according to system conditions. The key-equation for the Span & Wagner EOS (SW-EOS) is given by:

$$\frac{p(\delta,\tau)}{\rho RT} = 1 + \delta\phi_\delta^r \tag{6}$$

where ρ is density, $\delta = \rho/\rho c$, $\tau = T_c/T$ and $\phi_\delta^r = \left[\partial\phi/\partial\delta\right]_\tau$ is the derivative of the dimensionless Helmholtz free energy with respect to reduced density δ and is defined in Span & Wagner (1996). Both, DMW-EOS and SW-EOS, have to be solved iteratively. A method known as the van Wijngaarden-Dekker-Brent method (Brent, 1971) turned out to be the most applicable approach to find the desired roots of (4) and (6), since it guarantees convergence as long as the result lies within a defined interval. Due to iteration loops, the computational costs for solving DMW-EOS

and SW-EOS are much higher than for PR-EOS. Depending on the pT-region of the phase diagram, the computing time for the latter two equations may be ten to twenty times higher then for the first one (at "ideal" gas state, convergence can be reached much faster than in the vicinity of the critical point or at the line of vaporization).

To show the accuracies of all four EOSs, we compare their outcome with a total of 1465 density measurement datasets of CO_2 from various authors, see Table 1. Some of these datasets have also been used from the developers of DMW-EOS and SW-EOS to fit their correlations or to check their results. For better comparability, we classified the datasets into four regions defined by: $T < T_c$ and $p < p_{vap}(T)$ for the vapour region, $T < T_c$ and $p > p_{vap}(T)$ for the liquid region, $T > T_c$ and $p < p_c$ for gas as well as $T > T_c$ and $p > p_c$ for supercritical region. $p_{vap}(T)$ is the vapour pressure, a function of T, representing the boundary between vapour and liquid region (Fig. 1). For the gas and supercritical regions, the scatter plots are shown in Figs 2 and 3. From Fig. 2 it can be seen, that for densities $\rho < 50$ kg/m^3 the ideal gas law gives satisfactory results compared to the measurements.

At standard temperature (T_n = 273.15 K), this value corresponds to a pressure up to $p \approx 2.0$ MPa. For higher densities, the ideal gas law predicted results show growing deviations. Surprisingly, the results of the general PR-EOS show better results than the parameter-fitted DMW-EOS in these both regions. In Table 2, the averaged absolute deviation AAD, and the root

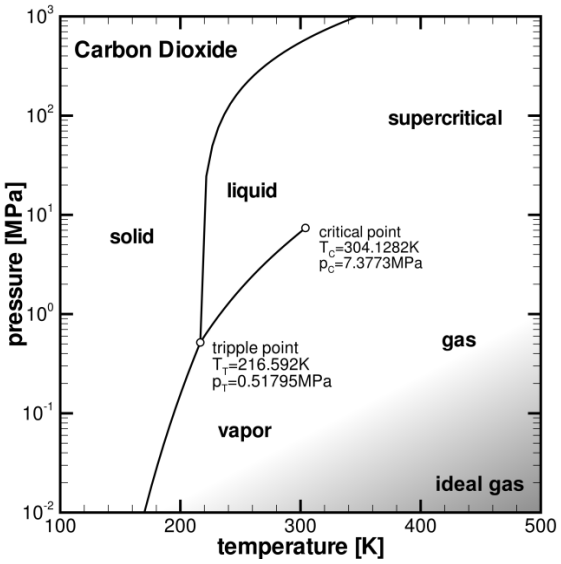

Fig. 1 Phase diagram of carbon dioxide.

Table 1 Sources, number as well as temperature and pressure intervals of the used pTρ datasets.

Source	n	ΔT [K]	Δp [MPa]	Source	n	ΔT [K]	Δp [MPa]
Ely *et al*. (1989)	61	250–330	2.2–35.5	Millat *et al*. (1987)	113	305–426	0.43–6.66
Gilgen *et al*. (1992)	69	280–310	1.0–13.5	Clifford *et al*. (1979)	22	301–303	0.6–5.9
Michels *et al*. (1957)	261	273–348	0.9–208.8	Fenghour *et al*. (1995)	120	330–698	3.0–34
Michels *et al*. (1962)	195	298–348	0.1–209.8	Guildner (1958)	22	304–348	0.22–30.4
Padua *et al*. (1994)	65	260–300	5.9–100	Kestin *et al*. (1980)	49	304	0.21–7.3
van der Gulik (1997)	158	220–308	0.5–100.5	Weber (1992)	12	320	0.14–6.0
Scott *et al*. (1983)	92	301–348	0.3–24.6	Duschek *et al*. (1990a,b)	226	280–320	0.5–9.0

n – number of datasets, ΔT – temperature range, Δp – pressure range

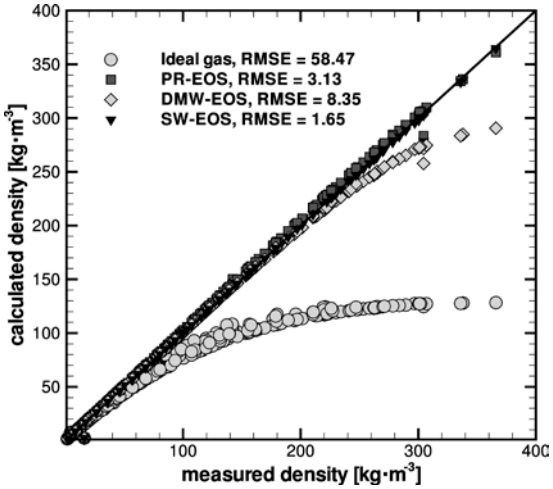

Fig. 2 Scatter-plot of measured and calculated density of CO_2 in the gas region ($T > T_c$, $p < p_c$).

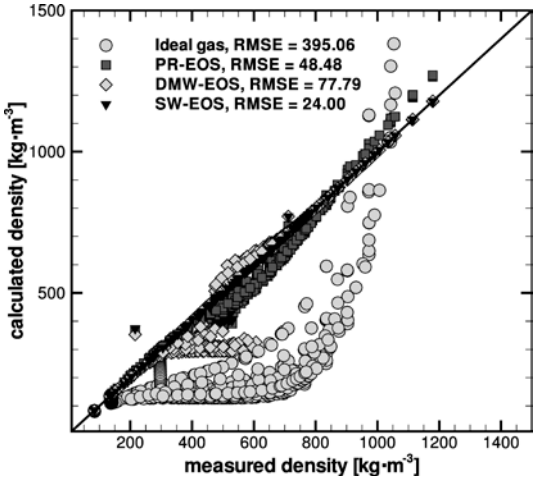

Fig. 3 Scatter-plot of measured and calculated density of CO_2 in the supercritical region ($T > T_c$, $p > p_c$).

Table 2 Averaged absolute deviation (AAD) and root of mean squared error (RMSE) of EOS-predicted densities from measurement data.

state	averaged absolute deviation (AAD) [%]			
	Ideal	PR	DMW	SW
SC	55.39	6.27	8.42	1.79
Gas	20.16	1.93	1.59	0.65
Liquid	63.79	10.31	1.19	0.06
Vapour	33.45	1.43	3.72	0.23
	Root of mean squared error (RMSE) [kg/m^3]			
	Ideal	PR	DMW	SW
SC	395.06	48.48	77.79	24.00
Gas	58.47	3.13	8.35	1.65
Liquid	612.51	189.5	62.78	1.29
Vapour	95.54	2.86	19.6	1.19

of the mean squared deviation RMSD is shown also for the liquid and the vapour region. From the data in this table we can see, that the DMW-EOS therefore gives much better results in the liquid region of the CO_2 phase diagram, where the cubic EOS gives no satisfactory results. The best

match to measured densities provides the fundamental SW-EOS. This result is no surprise, since SW-EOS uses the largest number of fitting parameters, and many of the datasets employed for this comparison has been used to tune the correlation to real-CO_2 behaviour. However, SW-EOS is the most precise equation of state for pure carbon dioxide available at this time.

NUMERICAL EXAMPLE

The hereafter presented example simulations consider a closed porous volume containing carbon dioxide at high pressure. At simulation start, the volume starts to be evacuated. According to the used EOS, the fluid pressure will drop while the gas expands. The observed pressure development in the volume is plotted for every simulation and can be compared.

Governing equation

The formulation for single-phase, compressible fluid flow in porous media derived by the continuity equation, has been implemented in OGS and reads:

$$\nabla \cdot \left(\frac{k\rho}{\mu} \nabla p \right) = n\rho\chi_f \frac{\partial p}{\partial t} + \rho q \tag{7}$$

with porosity n, time t, permeability k, viscosity μ, fluid density ρ, and a volumetric source or sink term q. Density is solved for pressure and temperature conditions according to the equations of state described in the last section. For the fluid compressibility we utilize the formulation:

$$\chi_f = \frac{1}{\rho} \frac{\partial \rho}{\partial p} \tag{8}$$

Benchmark test

We consider a one dimensional model domain of the porous volume, so gas flow occurs only in x-direction. A schematic of the domain is shown in Fig. 4. At the left boundary, a constant outlet pressure p_1 is applied, while flow through the right boundary is prohibited. An incompressible fluid would lead to an instantaneous dissipation of pressure, so the comparison to an exact solution proves the accuracy of the storage formulation. This test example simulates the evacuation of the volume assuming simplified conditions. To obtain an analytical solution for this problem, we consider a constant molar volume of the gas and compressibility according to ideal gas law. When density is not changing with pressure, the fluid compressibility χ becomes constant according to:

$$\chi_{\text{ideal}} = \frac{1}{\rho} \frac{M}{RT} \text{、} \tag{9}$$

Physically, this model setup is incorrect, since molar volume is not changing with decreasing pressure. But, this simplification is necessary to use equation (10) for benchmark purposes. This equation is an analytical solution for this problem, based on the solution for linear heat dissipation in a slab presented by Carslaw & Jaeger (1959):

$$p(x,t) = \frac{4p_0}{\pi} \sum_{i=0}^{\infty} \left\{ \frac{1}{2i+1} \sin\left[\frac{(2i+1)x\pi}{2L} \right] \exp\left[-ct \left(\frac{(2i+1)\pi}{2L} \right)^2 \right] \right\} \tag{10}$$

where p_0 is initial pressure, L is length of the domain and c is 1D-diffusivity defined by:

$$c = \frac{k}{\mu\phi\chi_{\text{ideal}}} \tag{11}$$

Figure 5 shows a comparison of analytical and numerical simulation. We see practically identical results for both solutions. This proves that the storage term for fluid compressibility implemented in equation (7) is correct.

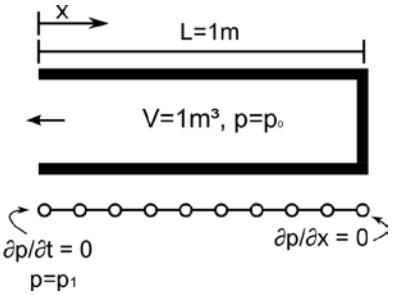

Fig. 4 Schematics of model domain and FE-mesh of benchmark test and comparative simulations.

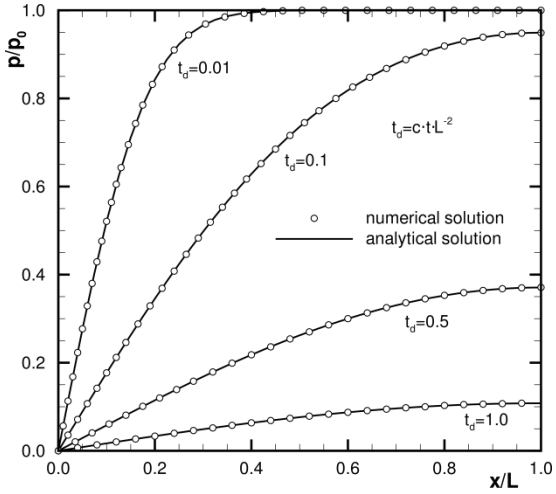

Fig. 5 Dimensionless comparison of analytical and numerical solutions of the benchmark test example.

Comparative simulations

Using the same model geometry as in the benchmark test (Fig. 4), we consider a medium with a porosity of $n = 0.05$ and a permeability of $k = 1 \times 10^{-14}$ m^2. The simplification made in the last section (keeping density constant), will be avoided for the following comparative simulations.

Physically, gas expands at the cost of thermal energy, so the temperature of a system would reduce when pressure is decreasing (Singh *et al*., 2011). To constrain our comparison to density and compressibility, we consider isothermal conditions and keep the CO_2 temperature at constant 305 K, which is slightly above critical temperature. Furthermore, viscosity has been considered to be constant with $\mu = 1 \times 10^{-5}$ Pa s. Unlike from liquid to vapour, the passage from supercritical to gaseous state occurs without discontinuities in the EOS, i.e. there is no phase change.

The initial pressure in the domain is $p_0 = 10$ MPa, at simulation begin, a standard pressure ($p_1 = 0.1$ MPa) boundary condition is applied at the left boundary. To investigate the effects of real gas behaviour, we designed the model conditions in a way that the working fluid would change its state from supercritical to gas. Since the pressure gradient dp/dt drops very fast during a simulation, the time step size was chosen to increase, starting from $dt = 1 \times 10^{-3}$ s in the beginning to $dt = 1 \cdot \times 10^{2}$ s at the end of the simulation.

Using different EOS, an initial pressure of $p_0 = 10$ MPa corresponds to different initial masses of CO_2 within the volume. At this pressure, the ideal gas law predicts an initial mass of $m_0 = 173$ kg/m^3, while the real gas EOS provide values between $m_0 = 697$ kg/m^3 and m_0=750 kg/m^3 (see Fig. 9). In Fig. 6, the observed pressure at the point $x = 0.2$ m is plotted for all considered EOS. The differences between ideal and real gas behaviour are significant. The pressure curve produced by the ideal gas law drops faster than the remaining curves at the beginning of the simulation, although the absolute velocity is lower. The reason for this effect is that (a) the total amount of

"ideal" CO_2 mass is lower than in the real gas simulations (so less CO_2 had to flow out) and (b) the compressibility (compare Fig. 8) according to ideal gas law is higher than according to PR-EOS, DMW-EOS or SW-EOS (so a change of pressure results in a larger change of density).

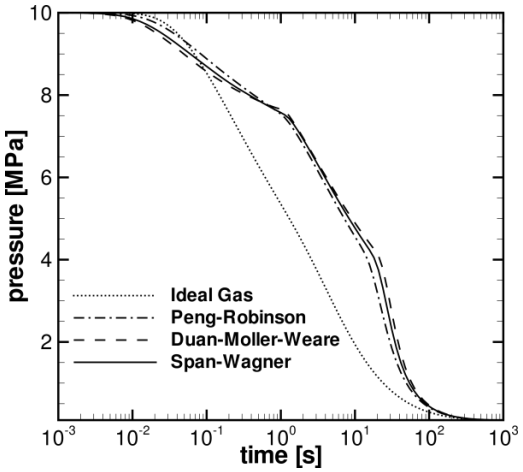

Fig. 6 Pressure decrease over time at observation point x = 0.2 m.

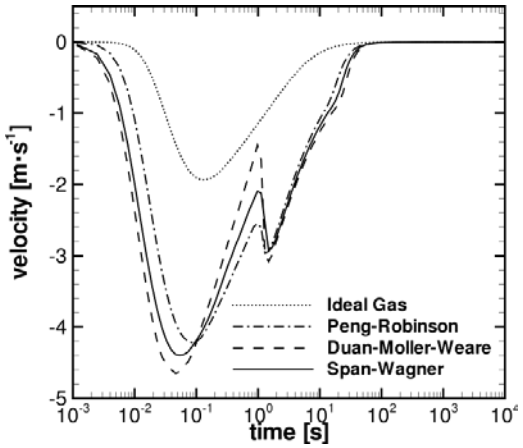

Fig. 7 Velocity development at x = 0.2 m.

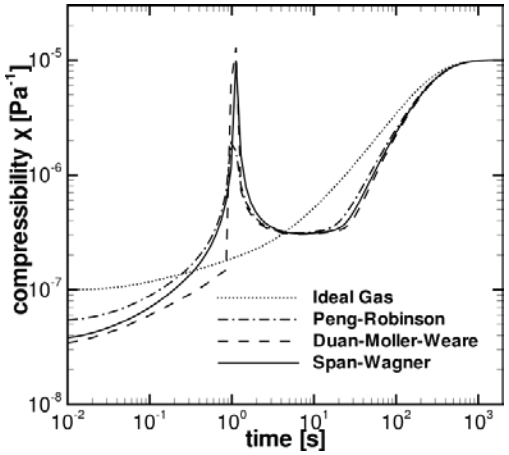

Fig. 8 Compressibility χ of CO_2 at x = 0.2 m *vs* time.

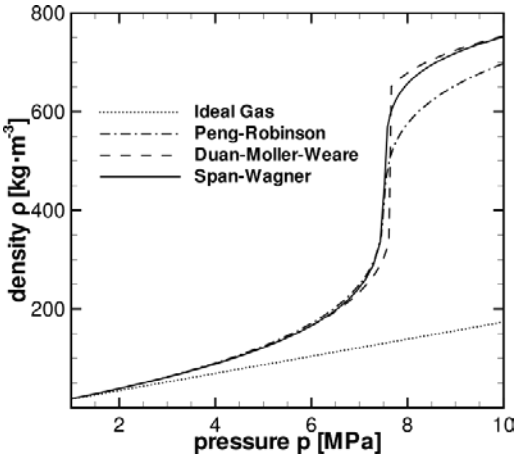

Fig. 9 Density of CO_2, derived by different EOS, at isothermal temperature t = 305 K.

The differences among the real gas EOS are less considerable. All three curves respond to the steep slope at $p \approx 7.5$ MPa of the density function, where the smooth passage from supercritical to gaseous state occurs. At this point (pseudocritical point), the compressibility rises significantly, which results in a faster pressure decrease. After t = 0.23 s, the pressure of the ideal gas drops to subcritical conditions. The real gas EOS reaches this point approximately at the same time (PR-EOS t = 1.21 s, DMW–EOS t = 1.37 s, SW–EOS t = 1.47 s).

SUMMARY AND CONCLUSION

We showed that, compared to measurement data, the EOS presented by Span & Wagner shows very accurate results. The virial Duan-Møller-Weare EOS produces acceptable densities of liquid CO_2, but shows larger deviations in the gas and vapour region than expected. Except for the liquid region, the two-parameter cubic EOS presented by Peng & Robinson provides admissible densities for all fluid phases of CO_2.

Since there are differences in density outcome, we performed numerical example simulations constrained to gas compressibility to see whether these differences are important or not. Regardless of its simplicity, the ideal gas law is a suitable EOS for CO_2 at low pressures. At the chosen temperature (T= 305 K) and above, CO_2 shows quasi-ideal behaviour up to pressures of $p \approx$ 2 MPa. For higher pressures, a real gas equation of state has to be used. Considering the constraint of compressibility, we can say that the advantage of performance when using a directly solvable cubic EOS justifies the slight differences in the simulation output. So, for the shown isothermal problem we designate the PR-EOS to be the most suitable equation of state.

For more complex problems, e.g. when non-isothermal effects, variable fluid properties or gas mixtures are considered, accuracy may play a more important role on the simulation results.

REFERENCES

Böttcher N., *et al*. (2011) Heat transport. In: *Benchmarks and Examples for Thermo-Hydro-Mechanical/Chemical (THM/C) Processes in Porous Media* (ed. by O. Kolditz). Springer.

Brent, R. P. (1971) An algorithm with guaranteed convergence for finding a zero of a function. *Computer J.* 14, 422–425.

Carslaw, H. S. & Jeager, J. C. (1959) *Conduction of Heat in Soils*, 2nd edn: Oxford University Press.

Clifford, A. A., Kestin, J. & Wakeham, W. A. (1979) Thermal conductivity of N_2, CH_4 and CO_2 at room temperature and at pressures up to 35MPa. *Physica A*, 97, 287–295.

Cohen, E. R. & Taylor, B. N. (1986) The 1986 Adjustment of the Fundamental Physical Constants, CODATA Bull. no. 63, Pergamon, Oxford.

Duan, Z., Møller, N. & Weare, J. H. (1992) An equation of state for the CH_4-CO_2-H_2O system: I. Pure systems from 0 to 1000°C and 0 to 8000 bar. *Geochimica et Cosmochimica Acta* 56, 2606–2617.

Duschek, W., Kleinrahm, R. & Wagner, W. (1990a) Measurement and correlation of the (pressure, density, temperature) relation of carbon dioxide. I. The homogeneous gas and liquid region in the temperature range from 217 K to 340 K at pressures up to 9 MPa. *J. Chem. Thermodynamics* 22, 827–840.

Duschek, W., Kleinrahm, R. & Wagner, W. (1990b) Measurement and correlation of the (pressure, density, temperature) relation of carbon dioxide. 11. Saturated-liquid and saturated-vapour densities and the vapour pressure along the entire coexistence curve. *J. Chem. Thermodynamics* 22, 841–864.

Ely, J. F., Haynes, W. M. & Bain, B.C. (1989) Isochoric (p, Vm,T) measurements on CO_2 and on ($0.982CO_2$+$O.018N_2$) from 250 to 330 K at pressures to 35 MPa. *J. Chem. Thermodynamics* 21, 979–984.

Fenghour, A., Wakeham, W. A. & Watson., J. T. R. (1995) Amount of substance density of CO2 at temperatures from 329 K to 698 K and pressures up to 34 MPa. *J. Chem. Thermodynamics*, 27, 219–223.

Fenghour, A., Wakeham, W. A. & Vesovic, V. (1998) The viscosity of carbon dioxide. *J. Phys. Chem. Ref. Data.* 27, 31–44.

Gilgen, R., Kleinrahm, R. & Wagner, W. (1992) Measurement of the (pressure, density, temperature) relation of sulfurhexafluoride in the homogeneous region from 321.15 K to 333.15 K and on the coexistence curve from 288.15 K to 315.15 K. *J. Chem. Thermodynamics* 24, 953–964.

Guildner, L. A. (1958) The thermal conductivity of carbon dioxide in the region of the critical point. *PNAS* 44(11), 1149–1153.

Kestin, J., Korfali, Ö. & Sengers, J. V. (1980) Density expansion of the viscosity of carbon dioxide near the critical temperature. *Physica A* 100, 335–348.

Michels, A., Sengers, J. V. & van der Gulik, P. S. (1957) The viscosity of carbon dioxide between 0°C and 75°C and at pressures up to 2000 atmospheres. *Physica* XXIII, 95–102.

Michels, A., Sengers, J. V. & van der Gulik, P.S (1962) The thermal conductivity of carbon dioxide in the critical region. *Physica* 28, 1216–1237.

Millat, J. Mustafa, M., Ross, M., Wakeham, W. A. & Zalaf, M. (1987) Thermal conductivity of argon, carbon dioxide and nitrous oxide. *Physica A*, 145, 461–497.

Padua, A., Wakeham, W. A. & Wilhelm, J. (1994) The viscosity of liquid carbon dioxide. *Int. J. Thermophysics* 15(5), 767–777.

Park, C.-H., Böttcher, N., Wang, W. & Kolditz, O. (2011) Are upwind techniques in multi-phase flow models necessary? *J. Comp. Physics*, doi: 10.1016/j.jcp.2011.07.030.

Peng, D. & Robinson, D. (1976) A new two-constant equation of state. *Ind. Engng Chem. Fundam*. 15, 59–64.

Pitzer, K. S. (1939) Corresponding states for perfect liquids. *J. Chem. Phys.* 7, 583–590.

Span, R. & Wagner, W. (1996) A new equation of state for carbon dioxide covering the fluid region from the triple-point temperature to 1100 K at pressures up to 800 MPa. *J. Phys. Chem. Ref. Data* 25(6), 1509–1596.

Scott, A., Johns, A. I. & Watson, J. T. R. (1983) Thermal conductivity of carbon dioxide in the temperature range 300-348 K and pressures up to 25 MPa. *J. Chem. Soc., Faraday Trans. 1* 79, 733–740.

Singh, A. K., Böttcher, N., Wang, W., Park, C.-H., Görke, U.-J. & Kolditz, O. (2011) Non-isothermal effects on two-phase flow in low-permeable porous media, *Energy Procedia* 4, 3889–3895, 10th International Conference on Greenhouse Gas Control Technologies, doi:10.1016/j.egypro.2011.02.326.

Stephan, K., Krauss, R. & Laesecke, A. (1987) Viscosity and thermal conductivity of nitrogen for a wide range of fluid states. *J. Phys. Chem. Ref. Data* 16(4), 993–1023.

van der Gulik, P. S. (1997) The viscosity of carbon dioxide in the liquid phase. *Physica* A, 238, 81–112.

Vesovic, V. & Wakeham, W. A., Olchowy, G. A., Sengers, J. V., Watson, J. T. R. & Millat, J. (1990) The transport properties of carbon dioxide. *J. Phys. Chem. Ref. Data* 19(3), 763–807.

Wang, W., Kosakowski, G. & Kolditz, O. (2009) A parallel finite element scheme for thermo-hydro-mechanical (THM) coupled problems in porous media. *Computers & Geosciences* 35(8), 1631–1641.

Weber, J. A. (1992) Measurements of the virial coefficients and equation of state of the carbon dioxide+ethane system in the supercritical region. *Int. J. Thermophysics* 13, 1011–1032.

Younglove, B. A. & Ely, J. F. (1987) Thermophysical properties of fluids. II. methane, ethane, propane, isobutane, and normal butane. *J. Phys. Chem. Ref. Data* 16(4), 577–798.